NAIC-ID(RS)T-0346-96

NATIONAL AIR INTELLIGENCE CENTER

PRELIMINARY RESEARCH FOR THE ACTIVE THIN MIRROR

by

Zeng Zhige, Ling Ning and Rao Xuejun

HUMAN TRANSLATION

NAIC-ID(RS)T-0346-96 4 October 1996

MICROFICHE NR:

PRELIMINARY RESEARCH FOR THE ACTIVE THIN MIRROR

By: Zeng Zhige, Ling Ning and Rao Xuejun

English pages: 12

Source: Qiangjiguang Yu Zizishu (High Power Laser and Particle Beams), Vol. 8, Nr. 1, February 1996; pp. 88-94

Country of origin: China
Translated by: Leo Kanner Associates
F33657-88-D-2188
Requester: NAIC/TATD/Bruce Armstrong
Approved for public release: distribution unlimited.

GRAPHICS DISCLAIMER

All figures, graphics, tables, equations, etc. merged into this translation were extracted from the best quality copy available.

Preliminary Research for the Active Thin Mirror

Zeng Zhige, Ling Ning and Rao Xuejun

(Institute of Optics & Electronics,
Chinese Academy of Sciences,Chengdu 610209)

Abstract: In this paper, the capabilities of the fitting aberration polynomials of two deformable mirrors which model active thin mirrors are calculated by using the finite element method, and fitting aberration experiments are introduced. The computation results and the experiment results agree very well.

Key words: active thin mirror, deformable mirror, finite element method, fitting aberration

0 Introduction

It is not unusual that in countries where large-scale ground-based telescopes and aerospace detectors are well developed active optics technology is used to correct the errors of the mirrors as well as to reduce their weight. The successful examples of this are VLT in ESO and the Hubble space telescope in the United States of America. Under the influence of gravity, temperature, etc., the optical accuracy of the large mirror surfaces may change, and an over-large mirror will almost inevitably produce larger errors through optical processing. In this case, application of the active thin mirror can not only reduce the weight, but also actively and controllably correct possible errors by using reinforced drivers and improve the optical surface, which proves to be particularly important for mirrors intended for use in aerospace detection.

The active thin mirror operates under the same principle as

the deformable reflector, i.e. a sufficient number of reinforced drivers, controlled by the control signal, are mounted on its back in a certain arrangement. These drivers are designed, by driving the mirror surface to generate deformation conjugated with the optical wavefront error, to adjust the optical image to an optimum quality. In our experiment, a 19-actuator (19 supporting points) deformable mirror and a 37-actuator (55 supporting points) deformable mirror were adopted to simulate the active thin mirror capabilities of compensating for various low-order aberrations.

The active thin mirror capability of fitting various aberration models represents its capability of compensating for a particular aberration model. The deformable mirror capability of fitting various aberration models is evaluated, based on the mean square root (RMS) and peak-valley value (P-V) of the residual surface shape, which is generated by the difference between the deformable mirror standard surface shape calculated by the quasi-Zernike polynomial (as shown in Table 1) aberration model, and the surface shape produced by the fitted aberration model.

With the help of the finite element simulation software, the simulation calculations of the deformable mirror fitting aberration can lead to a better understanding of the deformable mirror fitting capabilities as well as the stress distribution. Yet such calculations may overlook many factors that are unfavorable for the active optical devices in practical work, such as the change of temperature, variation of constraints, etc. Therefore, it is necessary to experimentally compare and verify the correctness of the simulation, and identify the effect of the constraints on the active optical devices.

Table 1. Quasi-Zernike Polynomial

Table 1 Quasi－Zernike Polynomial

wavefront aberration: $W=k\cdot\xi^{m}\cdot\ \cos(n\varphi+q\theta)$using	
$W=\ a$	constant
$+b\cdot\xi\cdot\cos(\varphi+\theta_0)$	wavefront tilt
$+c\cdot\xi^2$	longitudinal focus
$+d\cdot\xi^3\cdot\cos(\varphi+\theta_1)$	decentering coma(3rd order seidel)
$+e\cdot\xi^4$	spherical aberration(3rd order seidel)
$+f\cdot\xi^6$	5th order spherical aberration
$+g\cdot\xi^2\cdot\cos(2\varphi+\theta_2)$	astigmatism(3rd order seidel)
$+h\cdot\xi^3\cdot\cos(3\varphi+\theta_3)$	triangular coma
$+i\cdot\xi^4\cdot\cos(4\varphi+\theta_4)$	quadratic astigmatism
$+j\cdot\xi^4\cdot\cos(2\varphi+\theta_5)$	5th order astigmatism
$+k\cdot\xi^5\cdot\cos(\varphi+\theta_6)$	5th order coma

1. Computer Simulation of Deformable Mirror Fitting Low-order Aberration Models

The surface shapes of deformable mirrors are basically determined by the physical parameters of mirror surfaces and drivers, number and location of drivers, while the major stress change of the mirror surface takes place mainly at the junction between the mirror surface and the driver. The finite element models were built respectively for the 19-actuator and 33-actuator deformable mirrors as shown in Figs. 1 and 2. The 19-actuator deformable mirror contains 3802 mixed actuators and 3731 nodes while the 33-actuator deformable mirror--4559 mixed actuators and 4386 nodes.

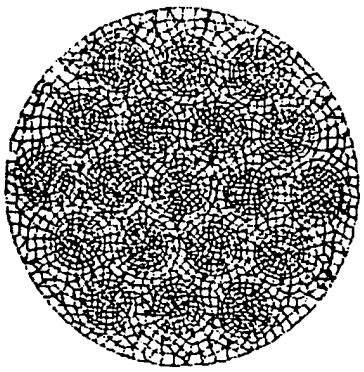

Fig. 1 Finite Element Model of
19-actuator Deformable Mirror

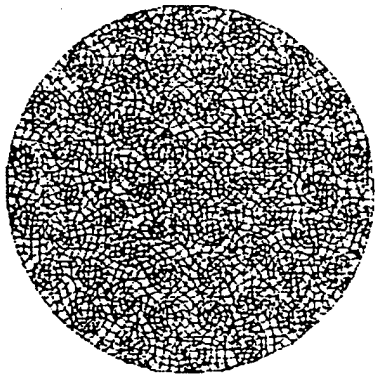

Fig. 2 Finite Element Model of
37-actuator Deformable Mirror

Figure 3 is a surface shape stereogram (948 sampling sites) of a quasi-Zernike polynomial aberration model fitted by the 37-actuator deformable mirror, derived from simulation calculations. The calculation results are listed in Table 2, and the surface shape RMS (mean square root) distribution is shown in Fig. 7 and 8.

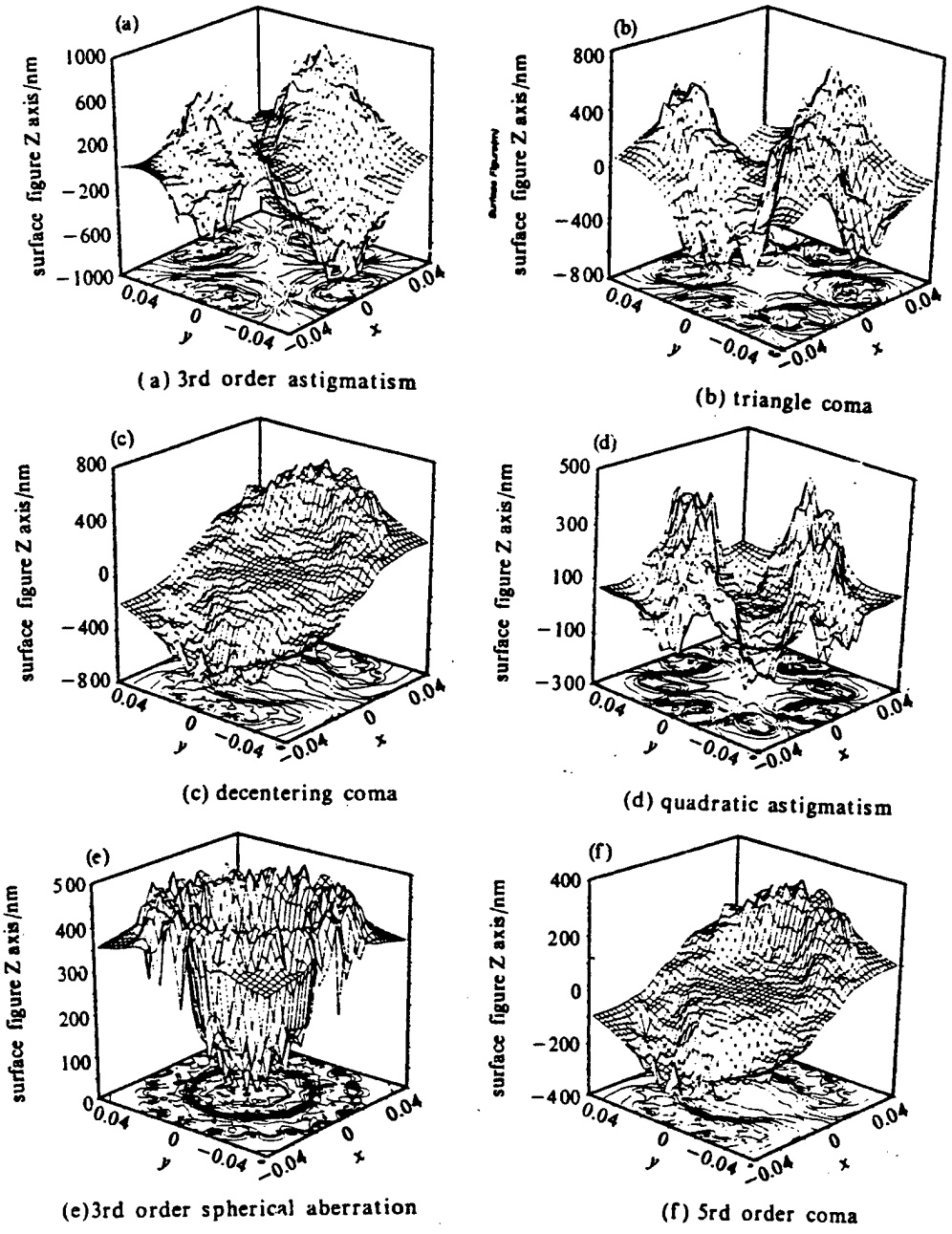

Fig 3 The mirror surface of fitting aberration by 37−actuator deformable mirror

Fig. 3. The Mirror Surface of Fitting Aberrations by 37-actuator Deformable Mirror

Table 2. The Fundamental Properties of a Deformable Mirror

deformable mirror	number of actuator	actuator arrangement	actuator distance	actuator material	surface quality	band
19-actuator	19	triangle	15mm	PZT	$<1/5\lambda$	>1kHz
37-actuator	37	radius	15mm	PZT	$<1/2\lambda$	>1kHz

2. Principle of Deformable Mirror Fitting Experiment

This experiment was designed to change, under the action of drivers struck by voltage from a high-voltage amplifier, the deformable mirror surface shape and fit different low space frequency aberration models--such as the quasi-Zernike polynomial (with +) as shown in Table 1, with the aberration function as:

$$W = k \cdot \xi^m \cos(n\varphi + q\theta)$$

where k is aberration function, m is radial order and n is angular order.

Figure 4 is a block diagram showing the principle of the aberration fitting experiment. In the first place, acquire the location data of drivers through the quasi-Zernike polynomial expression under the aberration surface shape to be fitted by the deformable mirror. Then, convert the displacement of drivers, in accordance with a certain relationship, into the voltage to be increased, and under the control of a microcomputer, impose different voltage values respectively to different drivers with a high-voltage amplifier so that the deformable mirror can generate an aberration surface shape to be fitted. Finally, judge whether or not the fitted surface shape has met the requirement by determining whether or not the RMS (mean square root value) of the residual surface shape produced by the difference between the standard aberration surface shape and the fitted surface shape is within the required range.

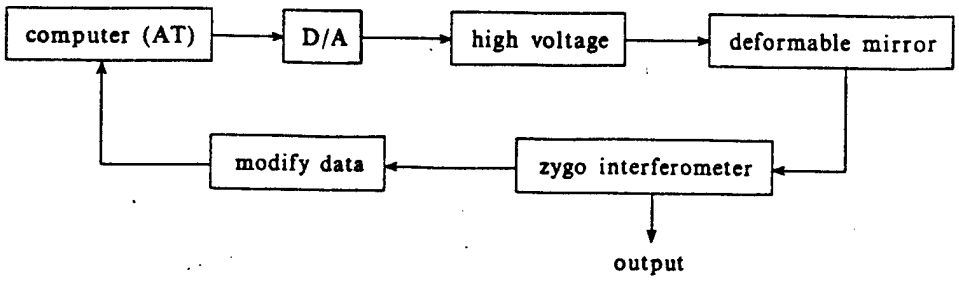

Fig. 4 Principle of the Fitting Aberration Experiment

3. Steps of Deformable Mirror Surface Shape Fitting Experiment

The different aberration surface shapes fitted by the deformable mirror are measured on a ZYGO digital interferometer. With wave surface subtraction functions, this device can measure the residual surface shape of the fitted aberration.

Two deformable mirrors were used in the experiment, 19-actuator and 37-actuator discrete piezoelectric deformable mirrors, whose parameters are listed in Table 2.

The basic steps of this experiment are listed as follows:

(1) Calculate, based on the algorithmic language, the final location of drivers when the mirror surface has been fitted into the quasi-Zernike polynomial aberration standard surface shape;

(2) Subtract the location of drivers for the original surface shape from that for the calculated standard surface shape and acquire the displacement of drivers needed for mirror surface fitting;

(3) Convert the displacement into the increase of voltage needed for the drivers to reach an ideal location;

(4) Measure and store the original surface shape data of the

deformable mirror by using the ZYGO interferometer;

(5) Under the control of a microcomputer, generate a stable voltage signal through D/A conversion, which is then amplified through a high-voltage amplifier and imposed on different drivers to cause deformation and drive the mirror surface to generate the fitted surface shape;

(6) Measure and store the fitted surface shape data in the interferometer;

(7) Acquire the residual surface shape by subtracting the fitted surface shape data from the theoretical surface shape data; and

(8) Repeat the above steps until the residual surface shape RMS value falls into the required range.

4. Measurements of Deformable Mirror Fitting Aberration

The surface contour and 3-D figures of various aberration models fitted by the 37-actuator deformable mirror and measured by the interferometer, are shown in Fig. 5 (a)-(f).

The residual surface shape RMS and P-V data, derived from the experiment on several low-order aberrations fitted by the 19-actuator and 37-actuator deformable mirrors, are listed in Table 3, and the fitted surface shape RMS values are given in Figs. 6 and 7.

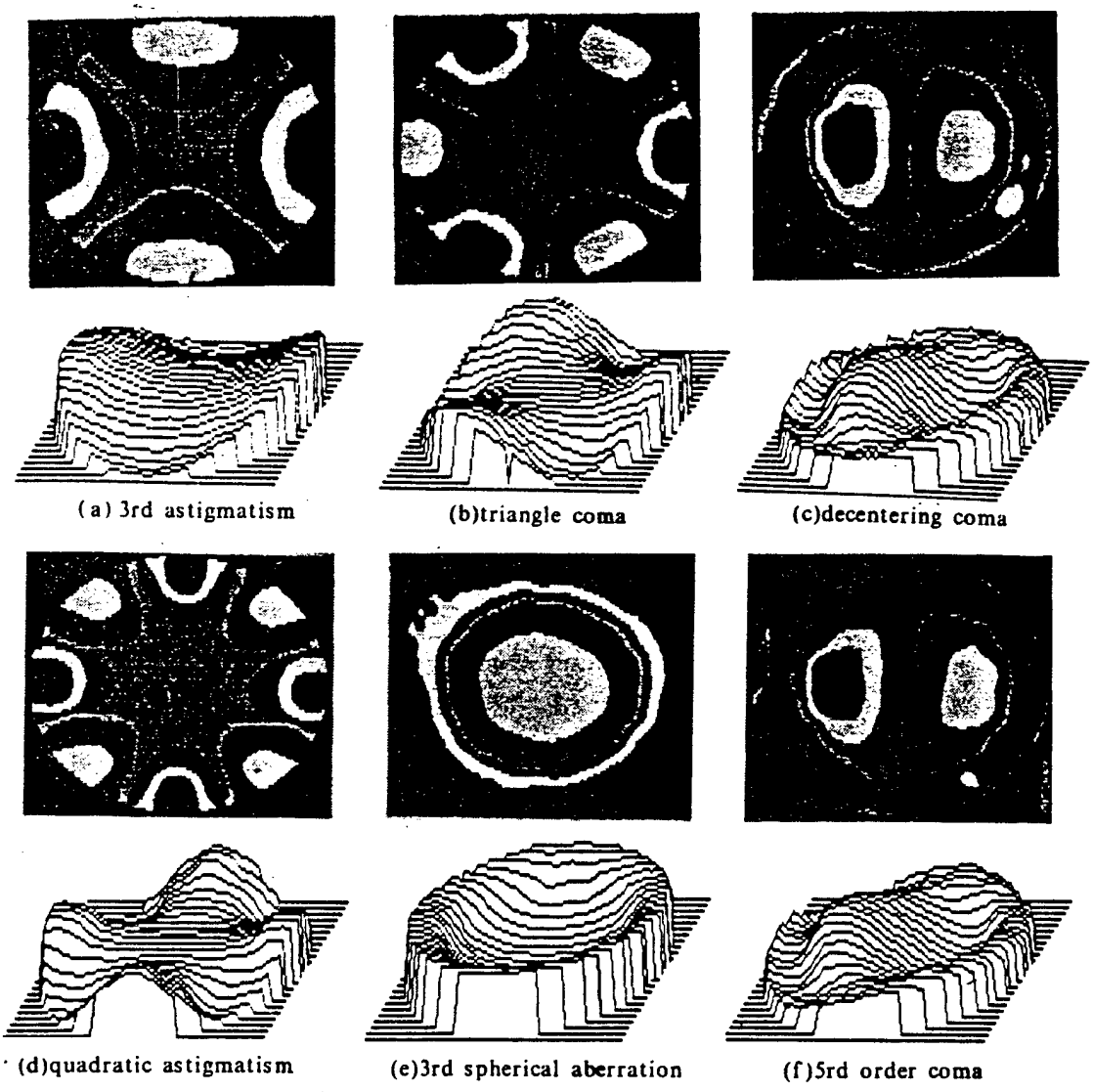

Fig. 5 The Surface Contour and the 3-D Figures of the 37-actuator Deformable Mirror

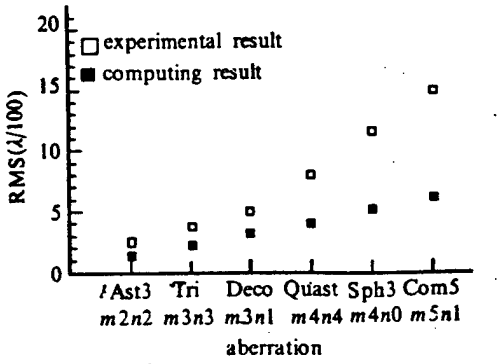

Fig 6 Fitting surface's RMS value of
19-actuator deformable mirror
■ the result of calculation
□ the result of experiment

Fig. 6. Fitting Surface's RMS Value of 19-actuator Deformable Mirror

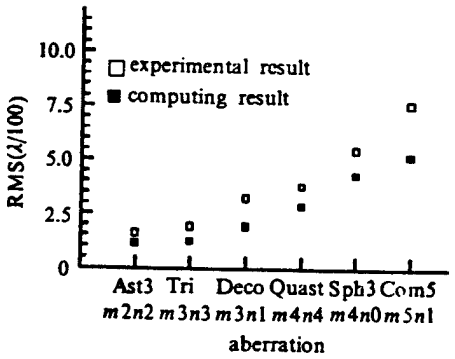

Fig 7 Fitting surface's RMS value of
37-actuator deformable mirror
■ the result of calculation
□ the result of experiment

Fig. 7. Fitting Surface's RMS Value of 37-actuator Deformable Mirror

Table 3 RMS Errors of Fitting Quasi-Zernike polynomial for 19- and 37-actuator Deformable Mirror

aberration	computing value /λ		experimental value /λ	
	19DM	37DM	19DM	37DM
3rd astigmatism($m2n2$)	1.5867e−2	1.3747e−2	2.7689e−2	1.8307e−2
triangular coma ($m3n3$)	2.3740e−2	1.5444e−2	4.0354e−2	2.2547e−2
decentering coma ($m3n1$)	3.5266e−2	2.3221e−2	5.3920e−2	3.6404e−2
quadratic astigmatism ($m4n4$)	4.3044e−2	3.2755e−2	8.9412e−2	4.1956e−2
3rd spherical aberration ($m4n0$)	5.7715e−2	4.8436e−2	1.2823e−1	6.1315e−2
5th order coma ($m5n1$)	6.7626e−2	5.4131e−2	1.6465e−1	8.5855e−2

5. Analysis of Deformable Mirror Aberration-Fitting Results

The following conclusions can be derived from the above experimental results for the same deformable mirror:

(1) The larger the number of drivers, the smaller the fitting errors. In other words, with the increase of the number of drivers, the deformable mirror can increase its capability of correcting the aberration models;

(2) The higher the radial order of the aberration model, the stronger the undulation of the aberration and accordingly, the stronger the undulation of the fitted surface shape, which is confirmed by both the experimental data and calculations; and

(3) In the aberration models with the same radial order, the higher the angular order, the smaller the fitting error, which conforms to the theoretical analysis and is demonstrated by the simulation calculations.

From the experimental data, the following conclusions can be arrived at concerning two different arrangements of drivers: the fitting error made by the 37-actuator deformable mirror with a radial arrangement of drivers turns out to be smaller than that from the 19-actuator deformable mirror with a triangle

arrangement of drivers. The major reason for this is that the number of drivers in the 37-actuator deformable mirror is larger than that in the 19-actuator one, which can verify the correctness of the simulation calculations.

6. Concluding Remarks

The result of the deformable mirror aberration model-fitting experiment shows that our simulation calculations are correct, which suggests that the active thin mirror technique is capable of correcting low-frequency aberrations and improving the quality of light beams. This income has eventually provided a theoretical basis and computing method for developing practical active thin mirrors.

References

1. Frank B. Ray and Yungtseng Chung. Applied Optics, 1985, 24(4):564-569.

2. DerShen Wan, Angle J R P, and Robert Parks E. Applied Optics, 1989, 28(2).

3. Washwell E R, Edwards D L, and Gelders A H. Processing of SPIE, Vol.365.

4. Aspinwall D M and Dotson R D. Processing of SPIE, Vol.365.

5. Richard R M and Malvick A J. Applied Optics, 1973, 12(6).

6. Fang Si. Research on Model control Deformable Mirror [Degree Dissertation], 1987.

7. Baifan Zhu. Principle and Application of Finite Element Method. Water Conservancy and Power Supply Press, 1979.

8. Yiwen Zhu et al. Finite Element Special CAD System ViziCad and Its Application. Beijing Si Tong Company, 1991.9.

This paper was received for revision on March 16, 1995.
The edited paper was received on October 10, 1995.